Springer

Journal of Mechanical Science and Technology 23 (2009) 442~451

Journal of Mechanical Science and Technology

www.springerlink.com/content/1738-494x
DOI 10.1007/s12206-008-1114-1

Topology optimization with displacement-based nonconforming finite elements for incompressible materials †

Gang-Won Jang[1] and Yoon Young Kim[2,*]

[1]*School of Mechanical and Automotive Engineering, Kunsan National University, Kunsan, Jeonbuk 573-701, Korea*
[2]*School of Mechanical and Aerospace Engineering and National Creative Research Initiatives Center for Multiscale Design, Seoul National University, Shinlim-Dong, San 56-1, Kwanak-Gu, Seoul 151-742, Korea*

(Manuscript Received March 17, 2008; Revised August 28, 2008; Accepted November 20, 2008)

Abstract

This investigation is concerned with the topology optimization using displacement-based nonconforming finite elements for problems involving incompressible materials. Although the topology optimization with mixed displacement-pressure elements was performed, a displacement-based approach can be an efficient alternative because it interpolates displacement only. After demonstrating the Poisson locking-free characteristics of the employed nonconforming finite elements by a simple patch test, the developed method is applied to solve the design problems of mounts involving incompressible solid or fluid. The numerical performance of the nonconforming elements in topology optimization was examined also with existing incompressible problems.

Keywords: Topology optimization; Nonconforming finite element; Incompressible material; Locking

1. Introduction

Most topology optimization techniques have been based on the displacement-based formulation because of simplicity in the formulation. However, standard displacement-based finite elements exhibit the so-called locking phenomenon when they are applied to the analysis of an incompressible material. Therefore, the topology optimization of a rubber-like incompressible material is also difficult with these elements. A remedy to such problems is to employ mixed finite elements. Sigmund and Clausen [1] used a mixed displacement-pressure formulation and assigned incompressibility to void elements to deal with topology optimization with pressure loads. Bruggi and Venini [2] presented a mixed formulation based on the triangular elements of Johnson and Mercier [3]. This investigation used element-wise linear and globally discontinuous displacement approximation and sub-element-wise linear stress approximation to pass the continuous and discrete inf-sup condition.

As an alternative approach to deal with the locking problem without resorting to a mixed formulation, one can use nonconforming elements. Brenner and Sung [4] approximated displacement field by triangular nonconforming elements with P_1 basis functions of Crouzeix and Raviart [5]. Triangular nonconforming elements are known to provide an efficient finite element space preserving discrete zero-divergence characteristics at each element. Rannacher and Turek [6] introduced rectangular nonconforming elements by rotating standard bilinear basis functions and showed that their nonconforming elements converge with optimal orders for uniform meshes. However, their elements lose optimality for quadrilateral partitions of an analysis domain. Douglas et al. [7] modified the element by Rannacher and Turek [6] by imposing orthogonalities along element edges and pre-

† This paper was recommended for publication in revised form by Associate Editor Tae Hee Lee

*Corresponding author. Tel.: +82 2 880 7154, Fax.: +82 2 883 1513
E-mail address: yykim@snu.ac.kr

sented nonconforming elements for quadrilaterals. They also applied nonconforming elements to solve the Maxwell [8] and Helmholtz equations [9]. Nonconforming elements were also used to solve wave propagation problems in viscoelastic media [10]. Lee et al. [11] showed the locking-free property of nonconforming elements in plane linear elasticity problems.

In topology optimization, nonconforming elements were used to suppress checkerboard patterns [12, 13]. Since the solution continuity of nonconforming elements is guaranteed only at midpoints of element edges in two-dimensional problems and at centers of element faces in three-dimensional problems, void elements of checkerboard patterns do not suffer from deformation constraints by diagonally positioned solid elements. In Reference [12], the homogenized stiffness of a checkerboard patch of nonconforming elements was shown to be merely twice the stiffness of void elements, while that of the conforming bilinear element is almost half of solid elements.

We consider nonconforming elements of Douglas et al. [7] and Lee et al. [11] to solve topology optimization problems of incompressible materials and investigate their numerical stability. Because the employed nonconforming elements are based on a displacement formulation, the standard formulation used for compressible materials can be directly used for incompressible problems. Furthermore, field consistency does not need to be considered. If a mixed formulation is used, on the other hand, one must satisfy field-consistency in displacement and stress interpolations [14]. Sigmund and Clausen [1] used linear displacement and constant pressure approximations and obtained stable solutions, but quadrilateral displacement and linear pressure approximation needs to be employed to obtain fully-stable solutions.

As done in Reference [1], the bulk and shear moduli are interpolated to represent material phases. In this work, the necessary and sufficient conditions for convergence of the nonconforming element are checked by the patch test, and the locking-free property of the element is examined with a test problem. More rigorous analysis may be found in References [7, 11]. For the topology optimization with nonconforming elements, the design of rubber-based mounts is considered. The underlying locking-free stable solution convergence of the nonconforming elements is tested also with existing incompressible design problems.

2. Characteristics of nonconforming finite elements

In this research, we adopt the quadrilateral nonconforming elements introduced by Lee et al. [11] whose shape functions are given as

$$\begin{aligned} N_1(\xi,\eta) &= \frac{1}{4}-\frac{1}{2}\eta-\frac{\theta_l(\xi)-\theta_l(\eta)}{4\theta_l(1)}, \\ N_2(\xi,\eta) &= \frac{1}{4}+\frac{1}{2}\xi+\frac{\theta_l(\xi)-\theta_l(\eta)}{4\theta_l(1)}, \\ N_3(\xi,\eta) &= \frac{1}{4}+\frac{1}{2}\eta-\frac{\theta_l(\xi)-\theta_l(\eta)}{4\theta_l(1)}, \\ N_4(\xi,\eta) &= \frac{1}{4}-\frac{1}{2}\xi+\frac{\theta_l(\xi)-\theta_l(\eta)}{4\theta_{(1)}}, \end{aligned} \tag{1}$$

where

$$\theta_l(t)=\begin{cases} t^2-\dfrac{5}{3}t^4, & l=1, \\ t^2-\dfrac{25}{6}t^4+\dfrac{7}{2}t^6, & l=2. \end{cases} \tag{2}$$

In Eq. (1), ξ and η denote element coordinates ($-1\le\xi,\eta\le 1$). Thus, the finite element space of the nonconforming element is

$$Q_l = \text{Span}\{\,1,\xi,\eta,\theta_l(\xi)-\theta_l(\eta)\}, l=1,2\,. \tag{3}$$

If a field variable u_e in the nonconforming quadrilateral element *e* is approximated as $u_e=\sum_i N_i U_i$ (N_i : shape function), the *i*-th degree of freedom U_i ($i=1,2,3,4$) denotes the average value of u_e on the *i*-th edge:

$$\begin{aligned} U_1 &= \frac{1}{2}\int_{-1}^{1} u_e\big|_{\eta=-1}\,d\xi, \\ U_2 &= \frac{1}{2}\int_{-1}^{1} u_e\big|_{\xi=1}\,d\eta, \\ U_3 &= \frac{1}{2}\int_{-1}^{1} u_e\big|_{\eta=1}\,d\xi, \\ U_4 &= \frac{1}{2}\int_{-1}^{1} u_e\big|_{\xi=-1}\,d\eta. \end{aligned} \tag{4}$$

Thus the continuity of the nonconforming elements along their interface is imposed by

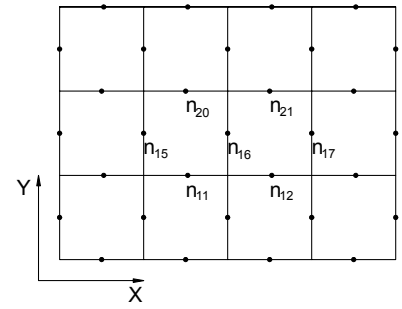

(a)

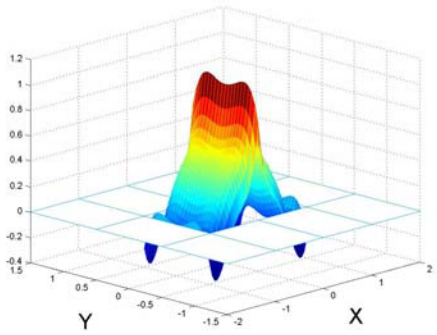

(b)

Fig. 1. A region discretized by 4×3 nonconforming elements: (a) node distribution and (b) shape functions associated with node 16.

$$\int_{\Gamma_{jk}} u_j d\Gamma = \int_{\Gamma_{jk}} u_k d\Gamma\,, \tag{5}$$

where Γ_{jk} denotes the element edge shared by element *j* and element *k*. Note that the degree of freedom U_i can be interpreted as the displacement at the midpoint of the corresponding edge. Because the continuity of nonconforming finite element solutions is guaranteed only at the midpoints of element edges, the continuity of the solution across interfaces between elements is released.

Fig. 1(a) illustrates a 4×3 mesh consisting of nonconforming elements. The elements have nodes located on the centers of element edges. Fig. 1(b) is a three-dimensional plot of the u field where $U_i = 0$ ($i = 1, 2, ...31, i \neq 16$) and $U_{16} = 1$. Note that along the edges of nodes 11, 12, 15, 17, 20 and 21, the u field is not continuous.

As the finite element mesh is refined, each element will approach a state of constant strain. To check the solution convergence of the nonconforming elements, let us consider a patch of nonconforming elements under the minimum number of displacement constraints to remove rigid body motions. If a patch of elements subject to nodal forces corresponding to a constant strain field can represent a state of constant strain, the finite elements are regarded to pass the convergence patch test and have at least $o(h)$ convergence for stresses even though the convergence is not monotonic (see, e.g., Reference [15]). Displacement continuity (or so-called compatibility) is not a necessary condition for the solution convergence of displacement-based finite elements.

For the patch test of the nonconforming elements, the following membrane problem is considered in a nonconforming finite element space NC^h:

Find $u \in NC^h$ such that

$$-T\nabla^2 u + ku - q = 0 \ \text{ in } \ \Omega \tag{6a}$$

with

$$u = \bar{u} \ \text{ on } \ \Gamma_u\,, \text{and } T\frac{\partial u}{\partial n} = \bar{t} \ \text{ on } \ \Gamma_t\,, \tag{6b}$$

where T, k and u denote the initial tension, the elastic foundation stiffness, and the displacement, respectively. In Eq. (6b), n denotes the direction normal to the boundary Γ_t. For the patch test, it is noted that a patch of elements has a constant strain field if $q = ku$. In this case, the Galerkin approximation of Eq. (6a) becomes

$$\int_{\Omega} v\left(-T\nabla^2 u\right) d\Omega = 0 \ \text{ for all } \ v \in NC^h\,, \tag{7}$$

which can be rewritten as a summation of integrations over each element domain Ω^e:

$$\sum_{e\in\tau_h} \int_{\Omega^e} v\left(-T\nabla^2 u\right) d\Omega = 0\,. \tag{8}$$

The integration by parts of Eq. (8) yields

$$\sum_{e\in\tau_h} \int_{\Omega^e} \left(T\nabla u\cdot\nabla v\right) d\Omega + \sum_{j,k\in\tau_h} \int_{\Gamma_{jk}} \left(v_j T\frac{\partial u}{\partial n_j} + v_k T\frac{\partial u}{\partial n_k} \right) d\Gamma = 0. \tag{9}$$

Because the finite element solution within each element is expressed in the space given by (3) having a space of a constant strain, the first term in Eq. (9) can represent a solution corresponding to a constant strain. Thus, the second term in Eq. (9) that denotes boundary forces resulting from displacement discontinuities along element edges must vanish or be ignored. Obviously, in case of conforming elements, the element boundary forces do not occur because $n_j = -n_k$ and $v_j = v_k$ on Γ_{jk}. Since the traction along element edge Γ_{jk} is constant, the element boundary force term in Eq. (9) becomes

$$\sum_{j,k\in\tau_h} \int_{\Gamma_{jk}} \left[\left(v_j - v_k \right) T \frac{\partial u}{\partial n_j} \right] d\Gamma \tag{10a}$$

$$= \sum_{j,k\in\tau_h} T \frac{\partial u}{\partial n_j} \int_{\Gamma_{jk}} \left(v_j - v_k \right) d\Gamma$$

$$= 0 . \tag{10b}$$

Eq. (10b) is due to Eq. (5). Accordingly, only the first term in Eq. (9) remains as the system equation. Therefore, the present nonconforming elements are shown to pass the patch test.

Now let us investigate how the nonconforming elements work in problems involving incompressible materials. The main difficulty of analyzing incompressible materials with displacement-based finite elements lies in inaccuracy in the prediction of mean stress or pressure. To demonstrate the locking-free property of the nonconforming element, its solution behavior will be examined when the volumetric part of strain becomes zero. The volumetric part of strain ε_v is related to mean pressure p as

$$p = K\varepsilon_v = K\left(\varepsilon_x + \varepsilon_y + \varepsilon_z \right), \tag{11}$$

where K is the bulk modulus of material and $\varepsilon_x, \varepsilon_y$ and ε_z are normal strains. For plain strain and three-dimensional problems,

$$K = \frac{E}{2(1+\nu)(1-2\nu)} \quad \text{and} \quad K = \frac{E}{3(1-2\nu)}, \tag{12}$$

Respectively, where E is Young's modulus and ν is Poisson's ratio. For mean pressure p to be finite in the limit of incompressibility ($\nu = 0.5$, i.e., $K \to \infty$), ε_v must be zero.

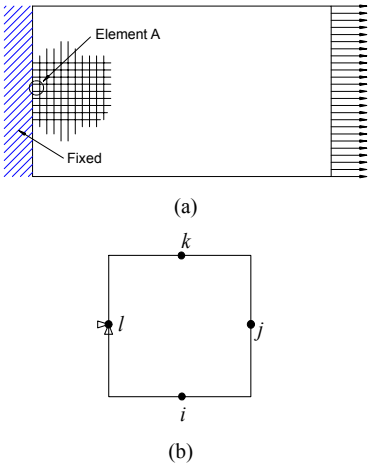

Fig. 2. A Poisson locking test problem: (a) a structure under uniform tensile load, and (b) boundary condition imposed on a nonconforming element (element A).

Fig. 2(a) describes a problem used to test the locking-free property of the nonconforming element. One end of a structure in Fig. 2(a) is fixed while the other end is subject to a uniform tensile load. The structure is discretized by the rectangular nonconforming elements, but the following analysis equally holds for general quadrilateral elements. For element A having nodes *i, j, k* and *l* shown in Fig. 2(a), we can express the volumetric strain ε_v as

$$\begin{aligned} \varepsilon_v = & -\frac{\partial\theta_l/\partial x}{4\theta_l(1)} U_{x,i} + \left(\frac{1}{2} + \frac{\partial\theta_l/\partial x}{4\theta_l(1)} \right) U_{x,j} \\ & - \frac{\partial\theta_l/\partial x}{4\theta_l(1)} U_{x,k} + \left(-\frac{1}{2} + \frac{\partial\theta_l/\partial x}{4\theta_l(1)} \right) U_{x,l} \\ & + \left(-\frac{1}{2} + \frac{\partial\theta_l/\partial y}{4\theta_l(1)} \right) U_{y,i} - \frac{\partial\theta_l/\partial y}{4\theta_l(1)} U_{y,j} \\ & + \left(\frac{1}{2} + \frac{\partial\theta_l/\partial y}{4\theta_l(1)} \right) U_{y,k} - \frac{\partial\theta_l/\partial y}{4\theta_l(1)} U_{y,l}, \end{aligned} \tag{13}$$

where $U_{\alpha,i}$ denotes the displacement component in the $\alpha-$direction ($\alpha = x, y$) of the *i*-th node. Imposing the constraint of zero volumetric strain to Eq. (13) yields

$$U_{x,j} - U_{x,l} - U_{y,i} + U_{y,k} = 0, \tag{14a}$$

$$-U_{x,i} + U_{x,j} - U_{x,k} + U_{x,k} = 0, \tag{14b}$$

$$U_{y,i} - U_{y,j} + U_{y,j} - U_{y,l} = 0 . \tag{14c}$$

Because $U_{x,l} = U_{y,l} = 0$ in element A due to the fixed boundary condition (see Fig. 2(b)), Eqs. (14) result in three independent linear equations with six nodal values. Therefore, the structure in Fig. 2(a) discretized by the nonconforming elements can deform freely under an external tensile load even in the limit of incompressibility. This analysis shows that the Poisson locking does not occur in the nonconforming element.

The convergence of the present nonconforming elements can be found in Reference [11]:

$$\| u - u_h \|_{1,h} \leq Ch \| u \|_2 , \tag{15}$$

where u and u_h denote the exact solution and the discretized solution in the nonconforming finite element space, respectively and h is the characteristic size of elements. In Eq. (15), the broken (energy) norm $\| \cdot \|_{1,h}$ excludes the effect of discontinuities along element boundaries (see [11] for the mathematical proof of Eq. (15)). Thus the analysis accuracy of nonconforming elements is dependent on the mesh density of topology optimization. Because the nonconforming elements have the Poisson-locking free property, the constant C in Eq. (15) is independent of material properties.

Fig. 3 shows the convergence of nonconforming elements; tip displacements of a cantilever structure whose free end is under a unit vertical force are plotted with respect to the number of elements. In the Fig., the convergence of mixed finite elements employing displacements and pressure as field variables (*u-p* formulation) is also plotted (4-node solid elements of ANSYS [16] are used for the calculation.) Although the accuracy of nonconforming elements in low mesh density is worse than that of mixed finite elements, the stable convergence expressed in Eq. (15) can be ascertained; the order of convergences for both cases are the same.

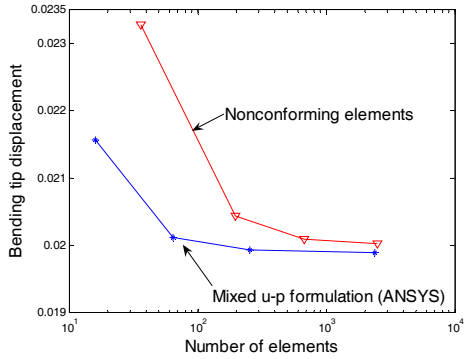

Fig. 3. Convergences of nonconforming elements and mixed finite elements for the tip displacement of a cantilever structure (a rectangular domain with $4\text{m} \times 1\text{m}$ assuming plane strain condition and incompressible material properties ($E = 10\text{kPa}$ and $\nu = 0.5$)).

Fig. 4 illustrates the deformed shape of nonconforming elements for the simple cantilever problem for Fig. 3. Note that the displacement continuity is preserved only at midpoints of element edges. Thus special attention needs to be paid when a displacement is used for the performance measure of optimization such as in compliant mechanism design problems. The displacements at the vertices of elements should not be used as performance measures of optimization.

3. Topology optimization formulation

The weak form of the governing equation for an elasticity problem is

$$\begin{aligned} &\int_\Omega \delta\varepsilon_{ij} C_{ijkl} \varepsilon_{kl} d\Omega - \int_\Omega \delta u_i f_i d\Omega \\ &- \int_{\Gamma_t} \delta u_i t_i d\Gamma = 0 \end{aligned} , \tag{16}$$

where ε_{ij} is the strain tensor, C_{ijkl}, the elasticity tensor, u_i, the displacement component, f_i, the body force component within the analysis domain Ω, and t_i, the prescribed traction on the boundary Γ_t. After discretization with the nonconforming finite elements, the weak form in Eq. (16) results in the following system of matrix equations:

$$\mathbf{KU} = \mathbf{F} , \tag{17}$$

where the stiffness matrix $\mathbf{K}$ and the force vector $\mathbf{F}$ are given as

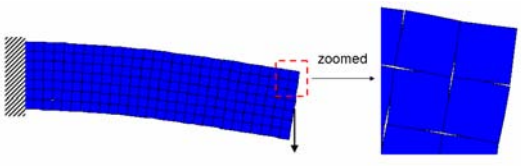

Fig. 4. Deformed shape of nonconforming finite elements.

$$\mathbf{K} = \sum_e \int_{\Omega^e} \mathbf{B}^T \mathbf{C}^e \mathbf{B} d\Omega \,, \tag{18}$$

$$\mathbf{F} = \sum_e \int_{\Omega^e} \mathbf{N}^T \mathbf{f} d\Omega \,. \tag{19}$$

In Eq. (18), $\mathbf{B}$ is the strain-displacement matrix consisting of derivatives of nonconforming shape functions $\mathbf{N}$, and $\mathbf{f}$ is the body force vector. The elasticity matrix $\mathbf{C}^e$ will be interpolated as a function of a design variable defined in each and every element. Note that the solution vector $\mathbf{U}$ in Eq. (17) consists of only displacement degrees of freedom.

Optimization formulation is given as

$$\underset{\rho}{\text{Minimize}}\ f = \mathbf{F}^T \mathbf{U} \,, \tag{20a}$$

subject to the volume constraint:

$$g = \frac{\sum_e \rho_e v_e}{V} \le \beta_{\text{solid}} \,, \tag{20b}$$

with

$$0 \le \rho_e \le 1 \,,$$

where ρ_e is a density design variable for an incompressible solid material. In Eqs. (20), v_e is the volume of the element *e*, and β_{solid} is the volume fraction of solid.

As suggested by Sigmund and Clausen [1], the bulk modulus *K* and shear modulus *G* will be used to represent the elasticity matrix. Therefore, *K* and *G* are interpolated as the functions of the element density design variables.

For topology optimization selecting an incompressible solid material state or void state for every element, the following interpolation is employed:

$$K(\rho_e) = K_{\text{void}} + (\rho_e)^p (K_{\text{solid}} - K_{\text{void}}) \,, \tag{21a}$$

$$G(\rho_e) = G_{\text{void}} + (\rho_e)^p (G_{\text{solid}} - G_{\text{void}}) \,, \tag{21b}$$

with

$$0 \le \rho_e \le 1 \,,$$

where K_{solid} and G_{solid} refer to the bulk modulus and the shear modulus of the original material, respectively and *p* denotes the penalty parameter. For plane strain problems, the elasticity matrix $\mathbf{C}^e$ in Eq. (18) in terms of *K* and *G* is written as

$$\mathbf{C}^e = \begin{bmatrix} K+G & K-G & \\ K-G & K+G & \\ & & G \end{bmatrix} . \tag{22}$$

Although K_{solid} should be infinite for incompressible materials, the value of K_{solid} that is 100 times larger than G_{solid} is used to simulate an incompressible material. If too large values of K_{solid} were used, elements having intermediate density values would exhibit incompressible behavior; it would become difficult to obtain distinct 0-1 density distributions. Bruggi and Venini [2] suggested larger interpolation exponents for the bulk modulus than for the shear modulus in order to obtain distinct 0-1 results. This technique is effective because Poisson's ratios corresponding to intermediate ρ_e values are evaluated to be very small and thus intermediate density elements do not posses large bulk modulus values. As a result, intermediate density elements are not favored during the topology optimization process. The use of a larger interpolation exponent for the bulk modulus than for the shear modulus is also known to be effective for problems with highly hydrostatic boundary conditions [2].

When designing a rubber-like structure containing fluid, instead of selecting void state, selecting fluid state should be formulated:

$$K(\rho_e) = K_{\text{solid}} = K_{\text{fluid}} \,, \tag{23a}$$

$$G(\rho_e) = G_{\text{fluid}} + (\rho_e)^p (G_{\text{solid}} - G_{\text{fluid}}) \,. \tag{23b}$$

In Eqs. (23), because elements in fluid state should also have incompressibility, their bulk modulus is set to be equal to that of an incompressible material, and thus only shear modulus is parameterized.

4. Design examples

To solve the topology optimization problems described in the previous section by a gradient-based optimization requires design sensitivity. Because the sensitivity analysis for a compliance minimization

problem is widely known, it will not be repeated here (see, e.g., Reference [17]). As an optimizer, the method of moving asymptotes by Svanberg [18] is used. To suppress the appearance of members with small sizes, the standard filtering technique [17] is used. Although the nonconforming elements are known to have the checkerboard-free property, members with small sizes could not be controlled in the test problems considered. Because a filter radius affects member sizes, small-sized members can be effectively suppressed with filters. After the convergence behavior of the nonconforming finite element based topology optimization with existing design examples is checked, the designs of a fluid-filled rubber will be solved. For θ_l in Eq. (2), we used the basis functions with $l=2$ for all problems solved here.

4.1 Verification with existing examples

Fig. 5 illustrates a bridge-like design domain with a center load. This problem was solved by Bruggi and Venini [2] using a mixed finite element approach. The domain boundaries interfacing with the hatch are fixed. The compliance minimization problem was solved for the two cases: a compressible material with $E=1$ and $\nu=0.25$ ($K_{\text{solid}}=0.8$ and $G_{\text{solid}}=0.4$) and an incompressible material with $E=1$ and $\nu\approx 0.5$ ($K_{\text{solid}}=100$ and $G_{\text{solid}}=0.333$). In Eqs. (21), $K_{\text{void}}=G_{\text{void}}=0.001$ and $p=3$ were used. The volume usage was constrained to be smaller than 35% of the design domain. Only half of the domain was analyzed with an 80×80 mesh. Therefore, 6,400 design variables were used for optimization.

The optimized results for compressible and incompressible materials are shown in Figs. 6 (a) and (b), respectively.

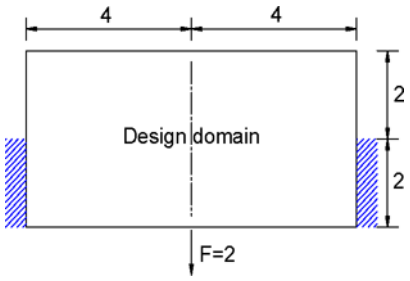

Fig. 5. Problem definition of a bridge-like structure.

Compared to the result for a compressible material, the result for an incompressible material has a higher upper arch, which indicates the structure takes advantage of material incompressibility. This fact can be also checked by examining the optimization value of compliance f_{opt}: $f_{\text{opt}}=11.956$ for the compressible case and $f_{\text{opt}}=9.114$ for the incompressible

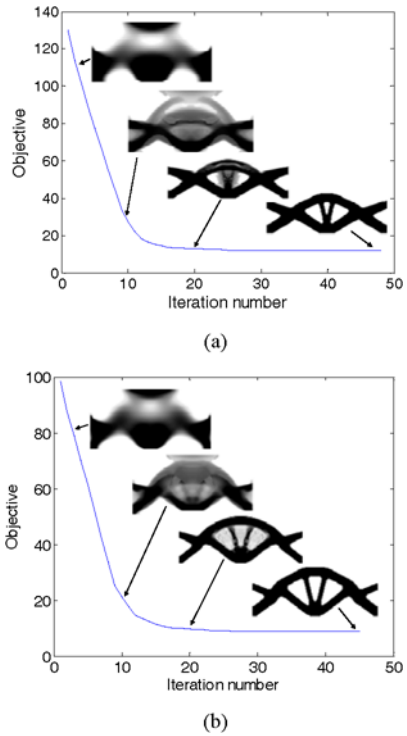

Fig. 6. Optimization history for the problem in Fig. 3 for (a) compressible material ($K_{\text{solid}}=0.8$, $G_{\text{solid}}=0.4$), and (b) incompressible material ($K_{\text{solid}}=100$, $G_{\text{solid}}=0.333$).

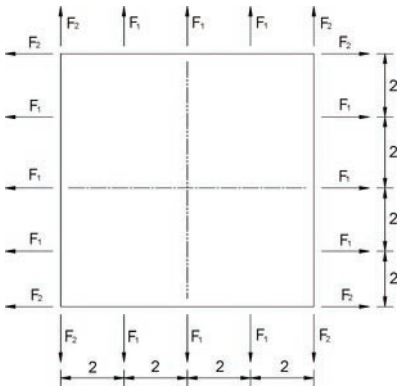

Fig. 7. Problem definition with nearly-isotropic loads ($F_1=2$, $F_2=1$).

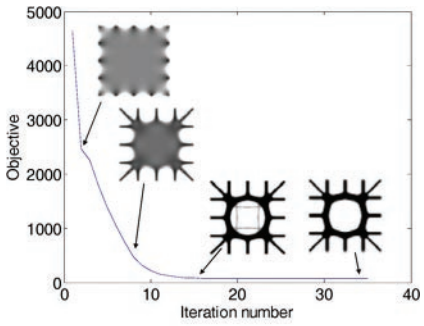

(a)

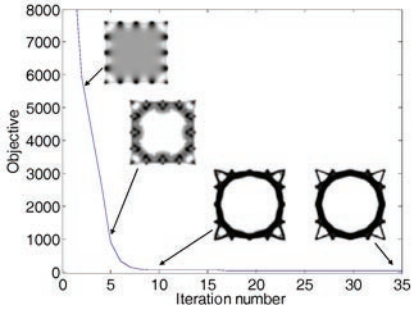

(b)

Fig. 8. Optimization history for the problem in Fig. 5 for (a) compressible material ($K_{\text{solid}} = 0.8$ and $G_{\text{solid}} = 0.4$), and (b) incompressible material ($K_{\text{solid}} = 30$, $G_{\text{solid}} = 0.333$).

case. The present result by the nonconforming displacement-based finite element approach with the incompressible material in Fig. 6(b) has almost an identical configuration to the result obtained by the mixed finite element approach [2].

In Fig. 7, a design domain of a structure subject to nearly-isotropic loads is illustrated. The material properties in the previous problem are used for optimization. A quarter of the design domain is discretized by 80×80 elements. Because the structure is under nearly isotropic loads, the elements apart from boundaries have almost the same deformations and thus almost the same sensitivities. Therefore, intermediate design variables would appear at the end of optimization unless a large penalty value for K is used. Also, as was suggested by Bruggi and Venini [2], we used different penalty exponents for the bulk and shear moduli: $p = 12$ for the bulk modulus and $p = 3$ for the shear modulus in Eqs. (21).

Fig. 8 compares the optimized results for the volume constraint of 35%. The optimized layout for a compressible material carries the external loads by the longitudinal stiffness of straight members that are

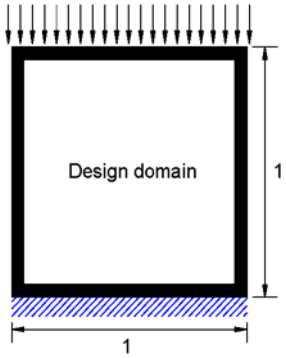

Fig. 9. Problem definition of a fluid-rubber mount.

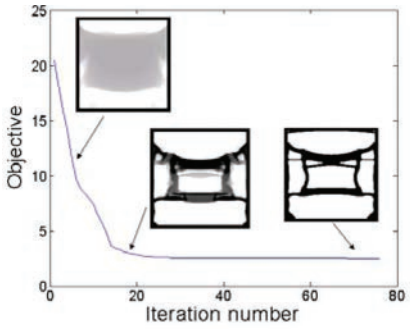

(a)

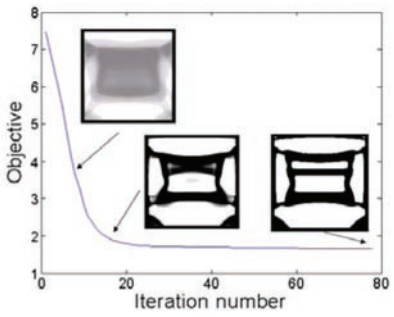

(b)

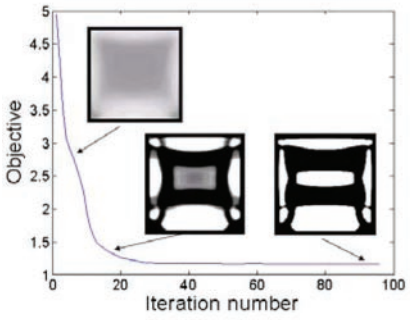

(c)

Fig. 10. Optimized fluid-rubber mounts: (a) 35%, (b) 45% and (c) 60% mass usage of a rubber (black: rubber, white: fluid).

reinforced by an internal circular ring. On the other hand, the layout for an incompressible material carries the loads mainly by a larger circular ring because of its strong resistance against compressibility. Obviously, the compliance of the incompressible case, $f_{\text{opt}} = 51.014$ turned out to be much smaller than the compliance of the compressible case, $f_{\text{opt}} = 73.432$.

4.2 Design of a fluid-filled rubber mount

The design optimization of a rubber mount of which internal region may be filled with fluid is now considered. Rubber mounts are structural elements to support vibrating structures such as engines. Although practical design of rubber mounts requires consideration of various factors (see, e.g., References [19, 20]), a simplified model will be considered to demonstrate the effectiveness of the present approach. Fig. 9 shows a design domain surrounded by thin rubber layers. The design domain will be filled with rubber and fluid. The fluid will be considered as an effective means to dissipate vibrating energy of a supported structure. The design problem set up here is the compliance minimization of the rubber mount with given volume ratios of rubber within the design domain. On the top edge of the support, a unit pressure is prescribed while the bottom edge is fixed. The half of the design domain and the surrounding non-design domain are discretized by 40×80 nonconforming elements. The interpolation scheme in Eqs. (23) is used to represent the rubber or fluid phase. The values of $K_{\text{solid}} = 100$, $G_{\text{solid}} = 0.3333$, $K_{\text{fluid}} = 100$ and $G_{\text{fluid}} = 0.001$ are used for Eqs. (23).

Fig. 10(a) shows the optimized rubber mount with the rubber volume constraint of 35%. The mount consists of three major regions, an upper chamber, a middle chamber and a lower chamber that are divided by arch-like rubber separators. Figs. 10(b) and (c) illustrate the optimized rubber mounts for 45% and 60% volume constraints, respectively. As the rubber volume ratio increases, mainly the middle chamber region is reinforced. To improve the vibration energy dissipation capability of the designed mount, one may consider small channels or holes between the fluid chambers. In that case, the optimized layouts obtained here could be used as good initial designs because mounts should have sufficient stiffness in addition to energy dissipation capability. The design of engine mounts by topology optimization considering energy dissipation as well as compliance will be a challenging problem.

5. Conclusions

Displacement-based nonconforming elements were employed for topological layout design optimization involving incompressible materials. Because the elements are free from the Poisson locking, no special technique such as the mixed formulation is needed to obtain stable solution convergence. The method was tested with new problems to design fluid-filled rubber mounts as well as existing design problems. Distinct 0-1 design variable distributions were obtained and stable solution convergence was found for all test problems. The locking-free analysis and numerical tests confirmed that the nonconforming element-based topology optimization method can be an effective alternative to the mixed element based topology optimization method.

Acknowledgments

The second author is supported by the National Creative Research Initiatives Program (Korea Science and Technology Foundation Grant No. 2007-019) contracted through the Institute of Advanced Machinery and Design at Seoul National University.

References

[1] O. Sigmund and P. M. Clausen, Topology optimization using a mixed formulation: an alternative way to solve pressure load problems, *Comput. Methods Appl. Mech. Engng.* 196 (2007) 1874-1889.

[2] M. Bruggi and P. Venini, Topology optimization of incompressible media using mixed finite elements, *Comput. Methods Appl. Mech. Engng.* 196 (2007) 3151-3164.

[3] C. Johnson and B. Mercier, Some equilibrium finite elements methods for two dimensional elasticity problems, *Numer. Math.* 30 (1978) 103-116.

[4] S. Brenner and L. Sung, Linear finite element methods for planar elasticity, *Math. Comp.* 59 (1992) 321-338.

[5] M. Crouzeix and P. -A. Raviart, Conforming and nonconforming finite element methods for solving the stationary Stokes equations, *RAIRO Math. Model. Numer. Anal.* 3 (1973) 33-75.

[6] R. Rannacher and S. Turek, Simple nonconforming quadrilateral Stokes element, *Numerical Methods*

for Partial Differential equations 8 (1972) 97-111.

[7] J. Jr. Douglas, J. E. Santos, D. Sheen and X. Ye, Nonconforming Galerkin methods based on quadrilateral elements for second order elliptic problems, *RAIRO Math. Model. Numer. Anal.* 33 (4) (1999) 747-770.

[8] J. Jr. Douglas, J. E. Santos and D. Sheen, A nonconforming mixed finite element methods for Maxwell's equations, *Math. Models Meth. Appl. Sci.* 10 (4) (2000) 593-613.

[9] J. Jr. Douglas, J. E. Santos and D. Sheen, Nonconforming Galerkin methods for the Helmholtz problem, *Numericla Methods for Partial Differential equations* 17 (2001) 475-494.

[10] P. M. Gauzellion, J. E. Santos and D. Sheen, Frequency domain wave propagation modeling in exploration seismology, *J. Comput. Acoust.* 9 (3) (2001) 941-955.

[11] C. -O. Lee, J. Lee and D. Sheen, A locking-free nonconforming finite element methods for planar linear elasticity, *Advances in Computational Mathematics* 19 (2003) 277-291.

[12] G. -W. Jang, J. J. Jeong, Y. Y. Kim, D. Sheen, C. Park and M. Kim, Checkerboard-free topology optimization using nonconforming finite elements, *Int. J. Numer. Meth. Engng* 57 (2003) 1717-1735.

[13] G. -W. Jang, S. Lee, Y. Y. Kim and D. Sheen, Topology optimization using nonconforming finite elements: three-dimensional case, *Int. J. Numer. Meth. Engng* 63 (2005) 859-875.

[14] O. C. Zienkiewicz and R. L. Taylor, The Finite Element Method, Volume 1: The Basis, Fifth edition, Butterworth- Heinemann, (2000).

[15] K. J. Bathe, Finite Element Procedures, Prentice-Hall, Inc., (1996).

[16] ANSYS Inc., ANSYS Structural Analysis Guide, (2007).

[17] M. P. Bendsøe and O. Sigmund, Topology Optimization, Theory, Methods and Applications, Springer, (2003).

[18] K. Svanberg, The method of moving asymptotes-a new method for structural optimization, *Int. J. Numer. Meth. Engng* 24 (1987) 359-373.

[19] W. C. Flower, Understanding hydraulic mounts for improved vehicle noise vibration and ride qualities, SAE Paper No. 850975, (1985).

[20] P. L. Graf and R. Shoureshi, Modeling and implementation of semi-active hydraulic engine mounts, *ASME Journal of Dynamic Systems, Measurement, and Control* 110 (1988) 422-429.

Gang-Won Jang received his M.S. degree in 2000, and Ph.D. degree in 2004, both from the School of Mechanical and Aerospace Engineering, Seoul National University, Seoul, Korea. He is currently an Assistant Professor at the School of Mechanical and Automotive Engineering, Kunsan National University, Jeonbuk, Korea. His current interest concerns topology optimization of multiphysics problems and thin-walled beam analysis.

Yoon Young Kim received his B.S. and M.S degrees from Seoul National University, Seoul, Korea, and the Ph.D. degree from Stanford University, Palo Alto, CA, in 1989. He has been on the faculty of the School of Mechanical and Aerospace Engineering, Seoul National University, since 1991. He is also the Director of the National Creative Research Initiatives Center for Multiscale Design. His main research field is the optimal design of multiphysics systems, mechanisms, and transducers. He has served as an editor of several Korean and international journals, and as an organizing committee member of several international conferences.